🔴 **COMMENTARY**

Playing the long game wins the cohesion–adhesion rivalry

Richard C. Remsing[a,1]

When a liquid meets a solid wall, the competition between cohesive fluid–fluid (*ff*) and adhesive fluid–wall (*fw*) interactions determines whether the liquid beads up into a droplet or spreads out over the surface. For typical liquids and moderate *fw* interactions, the surface is partially wet or partially dry. If the *fw* interactions decrease, the system will eventually undergo a surface phase transition to a state where the surface is dry—the liquid completely beads up into a spherical droplet, as is the case for ideal superhydrophobic water-repellant and self-cleaning surfaces. This is termed a drying transition. In contrast, if the *fw* interactions increase in strength, the system undergoes a surface phase transition to complete wetting—a wetting transition—in which the liquid completely spreads over the surface (1, 2). Our understanding of wetting and drying transitions stems from the seminal work of Nakanishi and Fisher (3, 4): a single class of surface phase transitions with wetting and drying becoming equivalent at the bulk critical point with temperature T_C. In PNAS, Evans et al. (5) predict 3 additional classes of surface phase diagrams, with the differences in the 4 total classes arising from the ranges of the *ff* and *fw* interactions (5).

A fundamental observable characterizing wetting/drying is the contact angle, θ, the angle of intersection between the solid wall (*w*) and the liquid–vapor (*l*–*v*) interface at the 3-phase contact line [see figure 1 of Evans et al. (5)]. The contact angle quantifies the balance of surface tensions, γ, where the 3 phases meet through Young's equation, $\gamma_{lv}\cos\theta = \gamma_{wv} - \gamma_{wl}$. Typical hydrophobic surfaces are characterized by $\theta > 90°$ and hydrophilic surfaces by $\theta < 90°$, with complete drying and wetting occurring at $\theta \to 180°$ and $\theta \to 0°$, respectively.

Physically, θ is a manifestation of the competition between *fw* and *ff* interactions, that is, adhesion versus cohesion. Evans et al. (5) answer the important question, "How do the ranges of these competing interactions affect wetting and drying transitions?" Most earlier work focused on cases where both *ff* and *fw* interactions were truncated at some length scale, such

that both were short-ranged (SR), often an approximation made to facilitate efficient numerical simulations. Evans et al. consider all 4 combinations of SR and long-ranged (LR) *ff* and *fw* interactions, and demonstrate—through analytic theory and subsequent validation via classical density functional theory and molecular simulation—that each combination leads to a different class of surface phase diagram (5): a) SR *ff* + LR *fw*, b) LR *ff* + LR *fw*, c) SR *ff* + SR *fw*, and d) LR *ff* + SR *fw*. The previously known class, in which wetting and drying are equivalent at T_C, is case c, where all interactions are SR. When LR interactions are present, wetting and drying are not equal at the bulk critical point, and a gap appears at T_C as a function of the *fw* interaction strength, ε_w; complete wetting and drying become fundamentally different.

Each surface phase diagram ultimately originates from the nature of the adhesive and cohesive interactions. The former are readily described by the *fw* interaction potential, $W(z)$. Cohesive forces arising from *ff* attractive interactions are more complex, but their average effects can be understood from a perspective dating back to van der Waals (2, 6, 7). In a uniform, bulk fluid, the vector sum of *ff* attractions is effectively zero in each configuration; fluid particles are pulled equally forcefully by their neighbors on every side. Thus, in bulk, attractive interactions do not alter the structure of the fluid and simply provide a uniform background potential in which the fluid particles move around.

Near a wall, the situation is vastly different. Fluid particles are still pulled by their neighbors' attractive forces, but because the symmetry of the system is broken, there is no cancelation in the direction of the surface normal, as schematically shown in Fig. 1A. Instead, a net cohesive force arises, opposing adhesion and pulling the fluid particles away from the surface. The net effects of *ff* cohesion can therefore be captured by an effective potential, $\varphi(z)$, which can be determined from a well-justified statistical mechanical theory (8, 9). This potential, $\varphi(z)$, encompasses the averaged effects of *ff* attractive interactions, such
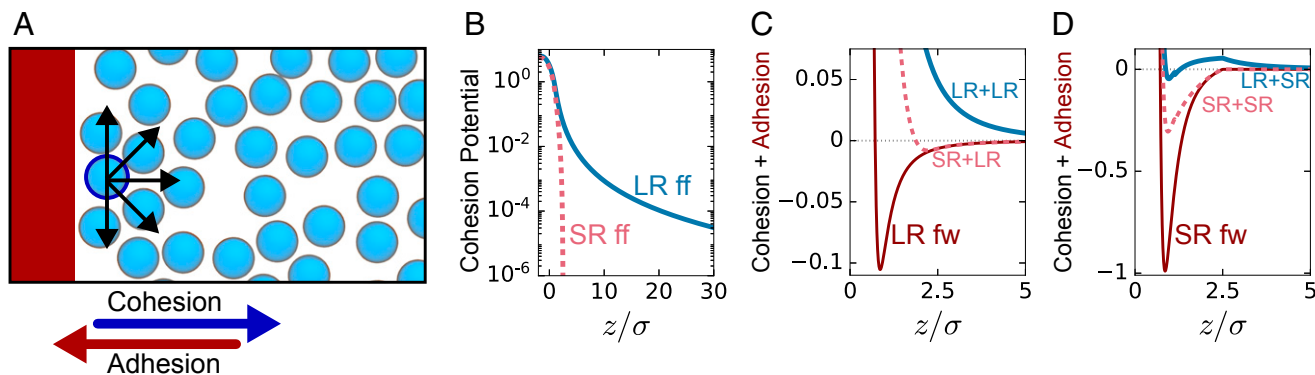
Fig. 1. (*A*) Schematic illustration of how cohesion arises from unbalanced fluid–fluid (*ff*) interactions at a liquid interface, highlighting the directionality of *ff* forces (arrows) felt by a single tagged particle (outlined). The net cohesive interaction opposes attractive adhesive interactions from a solid wall. (*B*) The effective potential leading to cohesion is repulsive, and its range depends on whether the *ff* interactions are short-ranged (SR) or long-ranged (LR). (*C* and *D*) The total potentials controlling drying and wetting is a sum of *ff* cohesion and fluid–wall (*fw*) adhesion potentials. In *C*, this is shown for a state point where LR + LR leaves the interface dry (phase diagram class b). Note the minimum and attractive tail in the total potential for SR *ff* interactions, indicating a lack of complete drying until the adhesive interactions tend to zero (class a). In *D*, the total potentials are shown for a SR *fw* adhesion, at a state of partial wetting for phase diagrams of class d. Note the maximum and repulsive tail in the LR cohesion + SR adhesion curve after the cutoff distance for adhesions, indicating partial wetting unless the adhesive interactions become infinitely strong.

that comparison of $\varphi(z)$ and $W(z)$ describes the quantitative balance between *ff* and *fw* interactions that underlie wetting and drying in the 4 classes of phase diagrams.

The effects of truncating the *ff* attractions are apparent in the effective cohesion potentials shown in Fig. 1*B* for both LR and SR interactions, with the latter truncated and shifted at 2.5σ, where σ is the diameter of a Lennard–Jones particle and $\varphi(z)$ was determined using a sharp-kink approximation for the density: $\rho(z) = 0$ for $z < 0$, $\rho(z) = \rho_B$ for $z > 0$. For LR *ff* interactions of the Lennard–Jones form, $\varphi_{LR}(z) \sim +\varepsilon\rho_B\sigma^6/6z^3$ at large distances, the same scaling form as the LR *fw* potential $W_{LR}(z) \sim -\varepsilon_w\varepsilon\sigma^3/z^3$, where ε is the energy scale for *ff* attractions. In this case, cohesion and adhesion can compete at all length scales, giving rise to class b phase diagrams. When adhesion dominates everywhere, e.g., large but finite ε_w, wetting occurs. When cohesion dominates everywhere, e.g., small but finite ε_w, drying occurs. The drying case is illustrated in Fig. 1*C* through the sum of cohesion and adhesion interactions, $\varphi_{LR}(z) + W_{LR}(z)$, which is repulsive for all z.

When the *ff* interactions are truncated at some finite distance, the cohesive interactions encompassed by $\varphi_{SR}(z)$ rapidly go to zero near the cutoff distance as shown in Fig. 1*B*. For phase diagrams of class a—SR *ff* and LR *fw*—when the *fw* interactions win out, partial and complete wetting can occur. However, because the *ff* potential is truncated, $\varphi_{SR}(z)$ is of finite range, there will necessarily always be a range of z where the fluid only feels the attractive potential $W_{LR}(z)$, and the width of the low-density vapor phase will always be finite for $\varepsilon_w > 0$. Thus, the drying transition can only occur for $\varepsilon_w \to 0$. For short-ranged *ff* and long-ranged *fw* interactions, cohesion never wins.

Similar arguments can be made for class d phase diagrams by exchanging the range of *ff* and *fw* interactions, Fig. 1*D*. The drying transition of this class mimics the wetting transition of class a, but with a long-ranged attractive potential replaced by a long-ranged repulsive potential. Interestingly, for this combination of interactions, the fluid can never completely wet the surface for finite adhesion. The repulsive $\varphi(z)$ persists after the *fw* potential is zero, favoring the vapor in this region, such that the width of the liquid phase remains finite unless $\varepsilon_w \to \infty$. For long-ranged *ff* and short-ranged *fw* interactions, adhesion never wins.

The discovery of these 3 classes of surface phase diagrams has profound consequences for the use of computer simulations in understanding physical systems. For efficiency, most molecular simulations employ truncated interaction potentials, especially between fluid particles, working under the assumption that the essential physics does not change. For a bulk fluid, such an assumption is valid. The bulk phase diagram remains qualitatively the same, with the location of the critical point and liquid densities shifting toward lower values, for example. At an interface, the neglect of long-ranged interactions changes even the qualitative behavior of the system. The work of Evans et al. highlights that most simulation studies of wetting and drying employing truncated interactions are not modeling the intended reality with long-ranged *ff* and/or *fw* interactions. Modeling long-ranged, power law interactions in interfacial geometries is a challenge, hence the oft-used truncation schemes, but advances in theoretical techniques for handling these potentials (8, 9) combined with efficient computational methods for probing surface thermodynamics (10–12) should provide a path forward to modeling real nonuniform systems.

While the focus of Evans et al. (5) is largely on macroscopic systems, their results will be important in a variety of important contexts at the nanoscale. Capillary evaporation and condensation in nanoconfined spaces between complex surfaces are thought to mediate biomolecular self-assembly processes (13), as well as the complex switching mechanisms of ion channels underlying biological temperature sensing (14), for example. Nanotextured superhydrophobic surfaces use patterning and confinement to reduce *fw* adhesion and push the system toward drying, and understanding the interplay of capillary evaporation and surface thermodynamics can be used to design robust superhydrophobic surfaces (15). Even at these small scales, macroscopic arguments involving surface tensions and the contact angle θ seem to describe the relevant capillary thermodynamics, although the kinetics of these processes is not and may require additional microscopic details (16, 17). Thus, one might expect that evidence for the different surface phase diagrams of Evans et al. may be observed even at the nanoscale and exploited for functionality through transitions in θ (18).

The final class of phase transitions described by Evans et al. (5) (class d) is particularly interesting. The combination of LR *ff* and SR *fw* interactions may be less relevant to most physical systems than its counterparts, but realizing such a situation could prove useful for functional materials. In nanoscale confinement, a drying transition cannot occur due to the finite size that confinement places on the growing film. However, because the drying transition in this case is first order, one may anticipate the existence of predrying transitions between thin and thick vapor films at the surface (19), which can occur in nanoconfinement, as is well known for analogous prewetting transitions (18, 20). One may envision designing a system situated near this transition, and small changes in T or ε_w would cause a finite-size vapor film to intervene between the liquid and the solid, in order to switch on and off processes like heat conduction, lubrication, or interfacial reactivity.

1 P. G. de Gennes, Wetting: Statics and dynamics. *Rev. Mod. Phys.* **57**, 827–863 (1985).

2 J. S. Rowlinson, B. Widom, *Molecular Theory of Capillarity* (Dover Publications, 2002).

3 H. Nakanishi, M. E. Fisher, Multicriticality of wetting, prewetting, and surface transitions. *Phys. Rev. Lett.* **49**, 1565 (1982).

4 M. E. Fisher, Walks, walls, wetting, and melting. *J. Stat. Phys.* **34**, 667–729 (1984).

5 R. Evans, M. C. Stewart, N. B. Wilding, A unified description of hydrophilic and superhydrophobic surfaces in terms of the wetting and drying transitions of liquids. *Proc. Natl. Acad. Sci. U.S.A.* **116**, 23901–23908 (2019).

6 B. Widom, Intermolecular forces and the nature of the liquid state: Liquids reflect in their bulk properties the attractions and repulsions of their constituent molecules. *Science* **157**, 375–382 (1967).

7 D. Chandler, J. D. Weeks, H. C. Andersen, van der Waals picture of liquids, solids, and phase transformations. *Science* **220**, 787–794 (1983).

8 J. D. Weeks, Connecting local structure to interface formation: A molecular scale van der Waals theory of nonuniform liquids. *Annu. Rev. Phys. Chem.* **53**, 533–562 (2002).

9 R. C. Remsing, S. Liu, J. D. Weeks, Long-ranged contributions to solvation free energies from theory and short-ranged models. *Proc. Natl. Acad. Sci. U.S.A.* **113**, 2819–2826 (2016).

10 H. Jiang, S. Fialoke, Z. Vicars, A. J. Patel, Characterizing surface wetting and interfacial properties using enhanced sampling (SWIPES). *Soft Matter* **15**, 860–869 (2019).

11 K. Jain, A. J. Schultz, J. R. Errington, Application of the interface potential approach for studying wetting behavior within a molecular dynamics framework. *J. Chem. Phys.* **150**, 204118 (2019).

12 R. Evans, N. B. Wilding, Quantifying density fluctuations in water at a hydrophobic surface: Evidence for critical drying. *Phys. Rev. Lett.* **115**, 016103 (2015).

13 B. J. Berne, J. D. Weeks, R. Zhou, Dewetting and hydrophobic interaction in physical and biological systems. *Annu. Rev. Phys. Chem.* **60**, 85–103 (2009).

14 M. A. Kasimova *et al.*, Ion channel sensing: Are fluctuations the crux of the matter? *J. Phys. Chem. Lett.* **9**, 1260–1264 (2018).

15 S. Prakash, E. Xi, A. J. Patel, Spontaneous recovery of superhydrophobicity on nanotextured surfaces. *Proc. Natl. Acad. Sci. U.S.A.* **113**, 5508–5513 (2016).

16 Y. E. Altabet, P. G. Debenedetti, Communication: Relationship between local structure and the stability of water in hydrophobic confinement. *J. Chem. Phys.* **147**, 241102 (2017).

17 G. Shrivastav, R. C. Remsing, H. K. Kashyap, Capillary evaporation of the ionic liquid [EMIM][BF$_4$] in nanoscale solvophobic confinement. *J. Chem. Phys.* **148**, 193810 (2018).

18 R. Evans, Fluids adsorbed in narrow pores: Phase equilibria and structure. *J. Phys. Condens. Matter* **2**, 8989–9007 (1990).

19 R. Pandit, M. Schick, M. Wortis, Systematics of multilayer adsorption phenomena on attractive substrates. *Phys. Rev. B Condens. Matter* **26**, 5112 (1982).

20 K. Binder, Modeling of wetting in restricted geometries. *Annu. Rev. Mater. Res.* **38**, 123–142 (2008).